

Ferrihollandite, $\text{BaMn}^{4+}_6\text{Fe}^{3+}_2\text{O}_{16}$, from Apuan Alps, Tuscany, Italy: description and crystal structure

CRISTIAN BIAGIONI*, CARMEN CAPALBO, MARCO LEZZERINI and MARCO PASERO

Dipartimento di Scienze della Terra, Università di Pisa, Via S. Maria 53, 56126 Pisa, Italy

*Corresponding author, e-mail: biagioni@dst.unipi.it

Abstract: The recent revisitation of the nomenclature of tunnel oxides belonging to the hollandite supergroup led to the definition of a new end-member, ferrihollandite, ideally $\text{BaMn}^{4+}_6\text{Fe}^{3+}_2\text{O}_{16}$. In particular, the type hollandite from Kajlidongri, Jhabua District, Madhya Pradesh, India, proved to be ferrihollandite. A new occurrence of ferrihollandite is here described from the manganese hydrothermal ores from Vagli, Apuan Alps, Tuscany, Italy, on the basis of chemical and X-ray diffraction data. Electron-microprobe data point to the following composition (in wt%): TiO_2 3.06, MnO_2 58.83, Mn_2O_3 8.64, Fe_2O_3 9.76, Al_2O_3 0.79, ZnO 0.03, SrO 2.77, BaO 14.63, Na_2O 0.09, K_2O 0.05, sum 98.65. The structural formula, based on 16 oxygen atoms and 8 octahedral cations per formula unit, is $(\text{Ba}_{0.793}\text{Sr}_{0.222}\text{Na}_{0.024}\text{K}_{0.009})_{\Sigma=1.048}(\text{Mn}^{4+}_{5.624}\text{Ti}_{0.318}\text{Fe}^{3+}_{1.016}\text{Mn}^{3+}_{0.910}\text{Al}_{0.129}\text{Zn}_{0.003})_{\Sigma=8.000}\text{O}_{16}$. The TG-DSC data show three main endothermic processes, related to the loss of water and the release of oxygen upon heating. The total mass loss is ~ 9.7 wt% in the temperature range between 25 and 1200 °C; the mass loss related to the release of water is ~ 1.5 wt%. Single-crystal X-ray diffraction study gives a monoclinic unit cell, a 10.0001(7), b 5.7465(4), c 9.8076(8) Å, β 90.713(2)°, V 563.56(2) Å³, space group $P2/n$. The crystal structure has been solved and refined on the basis of 1675 observed reflections, with a final $R_1 = 0.037$. The basic structural features of ferrihollandite are the same as the 2.9 Å hollandite-type compounds, but with long-range ordering of the tunnel cations. The occurrence of superstructure reflections could be related to the ordered sequence Ba–H₂O–Ba–H₂O within the tunnels.

Key-words: ferrihollandite, tunnel oxides, crystal structure, Apuan Alps, Tuscany, Italy.

1. Introduction

Minerals of the hollandite supergroup are tunnel oxides based on a 2×2 octahedral framework. They are divided into two groups, based on the dominant M cation within the octahedra: the coronadite group ($M = \text{Mn}^{4+}$) and the priderite group ($M = \text{Ti}^{4+}$). Within each group, mineral species are defined based on the combination of the dominant tunnel cation (A^{2+} or A^+) and the dominant charge-compensating cation (*i.e.* the M^{3+} or M^{2+} cation that partially substitutes for M^{4+} within the octahedra for charge-balance reasons).

Recently, the nomenclature of these minerals has been revised by Biagioni *et al.* (2013). During the reexamination of the available literature, some oddities in the eponymous mineral hollandite became apparent. Hollandite was first described by Fermor (1906), who studied a specimen from the manganese deposit of Kajlidongri, Jhabua District, Madhya Pradesh, India. The chemical composition, recalculated following the method suggested by Biagioni *et al.* (2013), gives the formula $\text{Ba}_{0.94}(\text{Mn}^{4+}_{6.12}\text{Fe}^{3+}_{1.08}\text{Mn}^{3+}_{0.64}\text{Al}_{0.15})_{\Sigma=7.99}\text{O}_{16}$; consequently, the type material is characterized by Ba^{2+} as the dominant tunnel cation and Fe^{3+} as the dominant charge-compensating cation. On the contrary, the name hollandite has been widely used to

describe a phase having Ba^{2+} as dominant tunnel cation and Mn^{3+} as dominant charge-compensating cation. Assuming that any combination of dominant tunnel cation and dominant charge-compensating cation represents a different mineral species, the hollandite described by Fermor (1906) and the various hollandite occurrences reported in the literature are actually two distinct minerals. In recognition of the fact that, in the common sense, the name “hollandite” points to a “manganese oxide”, and that actually at most occurrences hollandite has the end-member formula $\text{Ba}(\text{Mn}^{4+}_6\text{Mn}^{3+}_2)\text{O}_{16}$, it was agreed to keep the name hollandite for the Ba– Mn^{3+} end-member, and to introduce the new name ferrihollandite for the Ba– Fe^{3+} end-member. Those nomenclature changes have been approved by the IMA CNMNC (Biagioni *et al.*, 2013). It was also agreed that Kajlidongri (India) is the type locality for ferrihollandite, whereas the sample from Gowari Wadhona, Chindawara District, Madhya Pradesh, India (Miura, 1986) has been designated as neotype hollandite.

As a matter of fact, ferrihollandite is now a valid mineral species for which detailed mineralogical data are lacking: the early description by Fermor (1906), besides being given under the today incorrect name hollandite, is far from exhaustive. During our studies of the mineralogy of manganese hydrothermal deposits from Apuan Alps, we

identified a new occurrence of ferrihollandite. The aim of this paper is therefore the description of its occurrence, giving comprehensive chemical and structural data for this end-member of the hollandite supergroup.

2. Occurrence and mineral description

2.1. Occurrence of ferrihollandite

In the northern Apennines, manganese ores are known from different tectonic units. The most important ones are represented by braunite-bearing layers within hematite-rich cherts, belonging to the “Diaspri di Monte Alpe” Formation (Cabella *et al.*, 1998), in the ophiolitic sequences of Eastern Liguria. Small manganese ores were exploited also in the continental units belonging to the Tuscan Nappe and to the Apuane Unit. In the latter, four Mn deposits are known: Scortico (Di Sabatino, 1967), Monte Brugiana (Bonazzi *et al.*, 1992), Monte Corchia (Battaglia *et al.*, 1977; Franceschelli *et al.*, 1996), and Vagli (Perchiazzi & Biagioni, 2005; Biagioni *et al.*, 2009b).

At Vagli, braunite-bearing layers are hosted within hematite-rich metacherts of Middle Jurassic age known as “Diaspri” Formation. Braunite layers show the same deformation features as the country rocks and are conformable with the main field schistosity. Braunite layers are crosscut by quartz + calcite veins. Whereas braunite layers are probably syngenetic in origin, quartz + calcite veins formed during the Alpine tectono-metamorphic events.

The mineral assemblages in the braunite layers and in the quartz + calcite veins are different; ferrihollandite was found only in the latter kind of occurrence. The studied specimens come from small outcrops near the hamlet of Castagnola (latitude 44°06'N, longitude 10°15'E), some hundreds metres south of the village of Vagli di Sopra.

Ferrihollandite occurs as mm- to cm-sized black crystals, with a metallic lustre, usually embedded in quartz or calcite (Fig. 1); only very rarely, ferrihollandite was observed in small vugs. Crystals have a prismatic habit and are usually striated along [010], probably as a consequence of twinning on {101} or {10 $\bar{1}$ }, owing to the pseudo-tetragonal symmetry of ferrihollandite.

Ferrihollandite is associated with albite, braunite, clinocllore, hematite, muscovite, piemontite, rutile, titanite, and Mo-rich scheelite. Rarely, hollandite is strictly associated with rutile. Crystals of rutile have grown with their **c** axis parallel to the **b** axis of ferrihollandite and this geometric relationship can be the result of epitaxy owing to the structural similarities between rutile and 2 × 2 tunnel oxides.

Ferrihollandite is the third mineral species belonging to the hollandite supergroup identified from the Apuan Alps hydrothermal veins, the other two being hollandite from Monte Corchia (Orlandi, 1984; Franceschelli *et al.*, 1996) and mannardite from the Monte Arsiccio mine (Biagioni *et al.*, 2009a).

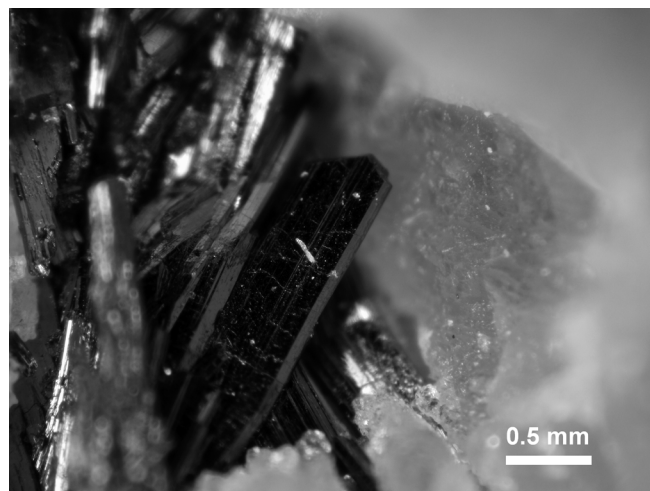


Fig. 1. Ferrihollandite, prismatic flattened crystals up to 2 mm long. Castagnola, Vagli di Sotto, Apuan Alps.

2.2. Chemical data

Preliminary qualitative chemical analyses were performed using a Philips XL30 scanning electron microscope equipped with an EDAX DX4 system. The only elements with $Z > 9$ detected in ferrihollandite are Ba, Mn, Fe, and minor Sr. Quantitative chemical analyses were carried out using an ARL-SEMQ electron-microprobe (Table 1). The operating conditions were: accelerating voltage 15 kV, beam current 20 nA, beam size 15 μm . Standards were: ilmenite (FeK α , TiK α), paracelsian (BaL α), microcline (AlK α , KK α), albite (NaK α), Sr-anortite (SrK α), spessartine (MnK α), and metallic Zn (ZnK α). Lead was sought but not detected.

The chemical formula of ferrihollandite, recalculated on the basis of 16 oxygen atoms and 8 octahedral cations per formula unit (pfu) is

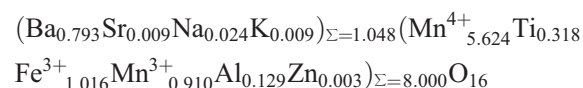


Table 1. Microprobe analyses (average of 17 spot analyses) of ferrihollandite.

Oxide	wt%	Range	e.s.d.
TiO ₂	3.06	2.70–3.50	0.30
MnO ₂ ^{tot}	68.35	67.58–70.53	0.75
MnO ₂	58.83		
Mn ₂ O ₃	8.64		
Fe ₂ O ₃	9.76	8.94–10.28	0.44
Al ₂ O ₃	0.79	0.67–1.21	0.12
ZnO	0.03	0.00–0.12	0.05
SrO	2.77	2.26–3.16	0.27
BaO	14.63	13.92–15.01	0.36
Na ₂ O	0.09	0.03–0.30	0.06
K ₂ O	0.05	0.03–0.12	0.02
Sum	98.65	97.40–99.77	0.74

The oxidation state of the reduced form of manganese was assumed as Mn^{3+} , in agreement with Post *et al.* (1982) and with the spectroscopic data (XANES) given by Manceau *et al.* (2012). All iron was assumed as trivalent, owing to the oxidized nature of the mineral assemblage, as proved by the widespread occurrence of hematite. Other mineralogical data pointing to a high $f\text{O}_2$ during the formation of this assemblage are represented by the occurrence of piemontite (Keskinen & Liou, 1979), the presence of braunite (Lucchetti *et al.*, 1988), the absence of FeCO_3 in solid solution with the carbonates, and the high Mo content (up to 23 mol% of powellite component) of scheelite (Hsu & Galli, 1973).

2.3. Thermo-gravimetric study

A powder sample of ferrihollandite (*ca.* 25 mg) was prepared for differential scanning calorimetry (DSC) and thermo-gravimetry (TG) analyses, in order to study the mass loss and verify the possible presence and amount of H_2O . Thermal analysis was performed by means of the TG-DSC equipment (TA Instruments, model Netzsch STA 449C Jupiter). The experimental conditions were: a) continuous heating from room temperature to 1200 °C, with a heating rate of 10 °C min^{-1} ; b) inert-gas (N_2) dynamic atmosphere (30 ml min^{-1}); c) alumina, top-opened crucibles; and d) no thermal pre-treatment of the samples.

As observed by previous authors (*e.g.*, Bish & Post, 1989), thermo-gravimetric data yielded mass losses considerably greater than expected from water loss only, due to the release of oxygen upon heating. Ferrihollandite from Vagli shows a total mass loss of ~ 9.7 wt% in the temperature range of 25–1200 °C (Fig. 2). Capalbo (2013) heated powdered samples of ferrihollandite at different temperatures, studying the heating products through powder X-ray diffraction; she observed a transformation from ferrihollandite to bixbyite (Mn_2O_3) above 700 °C and to hausmannite (MnMn_2O_4) above 800 °C. Consequently, the heating reduces Mn to lower valence states, giving rise to structural changes.

In the DSC curve, three main endothermic processes are evident between room temperature and 1000 °C; these processes are associated with mass losses, clearly shown in the DTG curve (Fig. 2). The first one (indicated as 1 on the DTG curve in Fig. 2), between 650 and 750 °C, corresponds to a mass loss of ~ 1 wt%; before 650 °C only a slight mass loss (~ 0.5 wt%) was observed. The second one (2) corresponds to a mass loss of ~ 3.4 wt%, whereas the third endothermic process is related to an additional mass loss (3) of 3.6 wt%. Above 1000 °C, an additional weak endothermic band occurs, corresponding to another mass loss of ~ 1.2 wt%.

2.4. Crystallography

Ferrihollandite was preliminary identified through powder X-ray diffraction, using a 114.6 mm diameter Gandolfi camera, with Ni-filtered $\text{CuK}\alpha$ radiation. Oscillation and Weissenberg photographs clearly indicated the occurrence of super-structure reflections with doubling of the b parameter, *i.e.* 5.8 Å (Fig. 3), with respect to the 2.9 Å unit-cell axis along the tunnel direction typical of the sub-structure of hollandite-supergroup phases.

Intensity data were collected using a Bruker Smart Breeze diffractometer, with air-cooled CCD detector and graphite-monochromatized $\text{MoK}\alpha$ radiation; the detector-to-crystal working distance was 50 mm; 978 frames were collected using φ and ω scan modes, in 0.5° slices, with an exposure time of 10 s per frame. The refined unit-cell parameters are a 10.0001(7), b 5.7465(4), c 9.8076(8) Å, β 90.713(4)°, V 563.56(2) Å³, space group $P2_1/n$. This space group is different from that indicated by Mukherjee (1960), *i.e.* $P2_1/n$, for a specimen of hollandite (actually ferrihollandite) from Kajlidongri, displaying the same unit-cell metrics with the 5.8 Å b parameter. In our dataset, the reflections 030, 050, and 070 violate the systematic absences in the reflection class $0k0$ for $k = 2n + 1$. Taking into account that Mukherjee (1960) used photographic methods for recording X-ray diffraction effects, it is possible that he was not able to observe the very weak reflections violating the systematic absences related to the 2_1 screw axis. As a matter of fact, Capalbo (2013) refined the

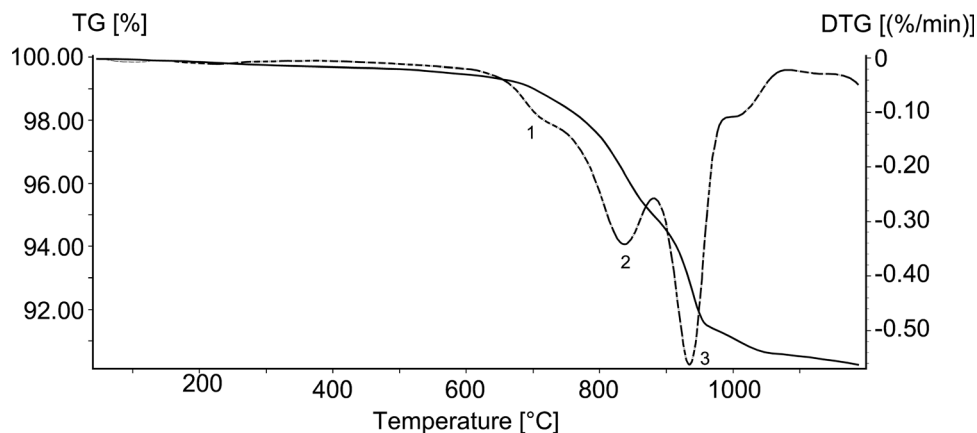


Fig. 2. TG and DTG curves (solid and dashed lines, respectively) for ferrihollandite from Vagli.

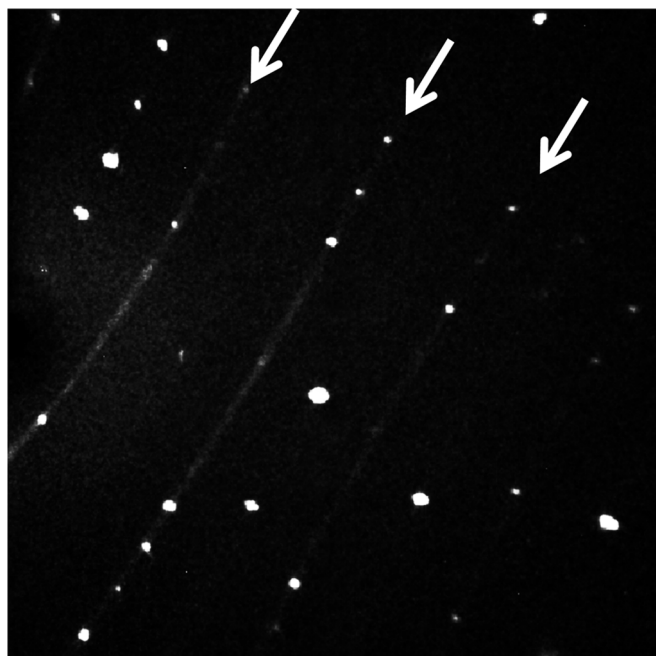


Fig. 3. An example of a single-crystal X-ray diffraction frame of ferrihollandite, collected with a Bruker Smart Breeze diffractometer. The image features (see arrows) k odd rows in which sharp reflections are superimposed on continuous streaks, leading to a 5.8 \AA b parameter.

crystal structure of ferrihollandite from Kajlidongri down to $R_1 = 0.032$ in the space group $P2_1/n$. Similarly, the space group symmetry of strontiomelane, given as $P2_1/n$ for the 5.8 \AA cell by Meisser *et al.* (1999), could be actually $P2_1/n$.

Intensity data were integrated and corrected for Lorentz, polarization, background effects, and absorption using the package of softwares APEX2 (Bruker AXS Inc., 2004). The structure was solved through direct methods using Shelxs-97 (Sheldrick, 2008). After locating the heavier atoms (Ba and Mn), oxygen atoms were found through difference-Fourier maps. The structure was refined by means of Shelx-97 (Sheldrick, 2008) up to $R_1 = 0.037 \%$ for 1675 observed reflections. Scattering curves for neutral atoms were taken from the *International Tables for X-ray Crystallography* (Wilson, 1992). Details of the data collection and crystal structure refinement are reported in Table 2.

3. Crystal-structure description

3.1. General organization

Atomic coordinates, displacement parameters, and selected bond distances are given in Tables 3, 4 and 5, respectively. Ferrihollandite displays a framework of octahedra linked together by edge-sharing forming double columns running along \mathbf{b} ; the columns share corners to give rise to a three-dimensional framework containing 2×2 tunnels (Fig. 4).

The crystal structure shows six independent cation sites, with six- and eight-fold coordination. The six-fold

Table 2. Crystal data and summary of parameters describing data collection and refinement for ferrihollandite.

Crystal data	
Crystal size (mm^3)	$0.31 \times 0.06 \times 0.05$
Cell setting, space group	Monoclinic, $P2_1/n$
Unit-cell dimensions	
a (\AA)	10.0001(7)
b (\AA)	5.7465(4)
c (\AA)	9.8076(8)
β ($^\circ$)	90.713(4)
V (\AA^3)	563.56
Z	2
Data collection and refinement	
Radiation type, (λ)	Mo $K\alpha$ (0.71073 \AA)
Temperature	room
Maximum observed 2θ ($^\circ$)	65.04
Measured reflections	6556
Unique reflections	2033
Reflections $F_o > 4\sigma F_o$	1675
R_{int}	0.0279
$R\sigma$	0.0284
Range of h, k, l	$-15 \leq h \leq 14$ $-8 \leq k \leq 8$ $-14 \leq l \leq 9$
$R_1 [F_o > 4\sigma F_o]$	0.0370
R_1 (all data)	0.0433
wR_2 (on F_o^2)	0.1216
Goof	1.180
Number of l.s. parameters	121
$\Delta\rho_{\text{max}}$ and $\Delta\rho_{\text{min}}$	3.63 (at 0.75 \AA from Ba2) -1.29 (at 0.62 \AA from Ba2)

coordinated sites are occupied by tetravalent transition elements (Mn^{4+} and minor Ti^{4+}), partly substituted by trivalent (Fe^{3+} , Mn^{3+} , and Al^{3+}) or bivalent (Zn^{2+}) cations. This substitution is paired with the introduction of alkaline or earth-alkaline metals in the tunnels.

3.2. Octahedral sites

Four independent octahedral sites occur in the crystal structure of ferrihollandite. Post *et al.* (1982) found that in hollandite and cryptomelane the octahedra are distorted, with the cations shifted along an octahedral triad axis, forming three longer and three shorter $M-O$ bonds. In priderite, on the contrary, the cations move along a tetrad axis. Some geometrical parameters used for a quantification of the size and the degree of distortion in the specimen from Vagli are given in Table 6: the measure of the distortion of a coordination polyhedron can be expressed, following Robinson *et al.* (1971), through two parameters, namely the bond angle variance σ^2 and the mean quadratic elongation λ . For a coordination polyhedron, $\sigma^2 = (1/11) \sum(\theta_i - 90^\circ)^2$ and $\lambda = 1/6 \sum(l_i - l_0)^2$, where θ_i are the bond angles, l_i are the bond distances, and l_0 is the bond distance for the ideal undistorted octahedron equal in volume to the one in question. Pasero (2005) used instead the parameter $\Delta = 1/6 \sum[(R_i - R)/R]^2$, where R_i is an individual $M-O$

Table 3. Atomic coordinates and displacement parameters (\AA^2) for ferrihollandite.

Site	Wyckoff site	Occupancy	x	y	z	U_{eq}
Ba1	2f	Ba _{0.218(1)}	$\frac{3}{4}$	0.3755(3)	$\frac{1}{4}$	0.0257(7)
Ba2	2f	Ba _{0.797(1)}	$\frac{3}{4}$	-0.12788(6)	$\frac{1}{4}$	0.0151(2)
Mn1	4g	Mn _{1.00}	0.10173(4)	0.62505(7)	0.08303(4)	0.0073(2)
Mn2	4g	Mn _{1.00}	0.41422(4)	0.37508(8)	0.09836(4)	0.0073(2)
Mn3	4g	Mn _{1.00}	0.41348(4)	-0.12490(8)	0.09585(4)	0.0068(2)
Mn4	4g	Mn _{1.00}	0.09917(4)	0.12489(7)	0.08389(4)	0.0067(2)
O1	4g	O _{1.00}	0.9069(2)	0.6296(3)	0.0497(2)	0.0095(4)
O2	4g	O _{1.00}	0.4559(2)	0.3710(4)	-0.0977(2)	0.0094(4)
O3	4g	O _{1.00}	0.5456(2)	0.1206(4)	0.0973(2)	0.0089(4)
O4	4g	O _{1.00}	0.4095(2)	-0.1240(3)	0.2900(2)	0.0098(4)
O5	4g	O _{1.00}	0.0916(2)	0.3734(3)	0.2082(2)	0.0100(4)
O6	4g	O _{1.00}	0.2900(2)	0.1246(3)	0.0754(2)	0.0100(4)
O7	4g	O _{1.00}	0.0928(2)	0.8790(4)	-0.0512(2)	0.0093(4)
O8	4g	O _{1.00}	0.2918(2)	0.6266(4)	0.0779(2)	0.0101(4)

Table 4. Anisotropic displacement parameters (\AA^2) for ferrihollandite.

Site	U_{11}	U_{22}	U_{33}	U_{23}	U_{13}	U_{12}
Ba1	0.0278(10)	0.0249(10)	0.0243(10)	0	0.0019(6)	0
Ba2	0.0177(2)	0.0130(2)	0.0146(2)	0	0.0007(1)	0
Mn1	0.0102(2)	0.0028(2)	0.0089(2)	0.0001(2)	0.0007(2)	0.0000(2)
Mn2	0.0108(2)	0.0031(2)	0.0080(2)	0.0001(2)	0.0010(2)	0.0002(2)
Mn3	0.0098(2)	0.0030(2)	0.0075(2)	0.0001(2)	0.0008(2)	0.0002(2)
Mn4	0.0097(2)	0.0028(2)	0.0078(2)	0.0001(2)	0.0008(2)	0.0001(2)
O1	0.0132(8)	0.0066(9)	0.0086(9)	0.0022(10)	-0.0004(7)	0.0024(8)
O2	0.0112(8)	0.0054(9)	0.0117(10)	0.0007(11)	-0.0009(7)	0.0024(8)
O3	0.0104(8)	0.0058(9)	0.0106(9)	0.0001(11)	-0.0006(7)	0.0012(8)
O4	0.0185(10)	0.0033(9)	0.0075(8)	-0.0003(11)	0.0010(7)	-0.0004(8)
O5	0.0188(10)	0.0029(9)	0.0082(9)	-0.0012(11)	0.0021(7)	-0.0002(8)
O6	0.0092(8)	0.0043(9)	0.0016(10)	-0.0005(11)	0.0003(7)	0.0001(8)
O7	0.0126(8)	0.0066(9)	0.0086(9)	0.0010(10)	-0.0008(7)	0.0024(8)
O8	0.0101(8)	0.0044(9)	0.0158(10)	-0.0004(11)	0.0001(7)	-0.0011(8)

Table 5. Selected bond distances (in \AA) in ferrihollandite.

Ba1	- O1	2.911(2) × 2	Mn1	- O5	1.901(2)	Mn3	- O8	1.882(2)
	- O2	2.916(2) × 2		- O8	1.905(2)		- O6	1.899(2)
	- O7	2.916(2) × 2		- O4	1.912(2)		- O4	1.903(2)
	- O3	2.918(2) × 2		- O1	1.960(2)		- O2	1.922(2)
	Average	2.915		- O7	1.970(2)		- O3	1.935(2)
			- O1	1.975(3)	- O3	1.941(2)		
			Average	1.937	Average	1.914		
Ba2	- O1	2.886(2) × 2	Mn2	- O5	1.898(3)	Mn4	- O5	1.881(2)
	- O2	2.889(2) × 2		- O8	1.900(2)		- O4	1.895(2)
	- O7	2.892(2) × 2		- O6	1.912(2)		- O6	1.914(2)
	- O3	2.897(2) × 2		- O2	1.956(2)		- O1	1.929(2)
	Average	2.891		- O3	1.964(2)		- O7	1.938(2)
			- O2	1.971(2)	- O7	1.944(3)		
			Average	1.934	Average	1.917		

bond distance and R is the average bond-length in each octahedron.

Mn1 and Mn2 octahedra are larger and more distorted than Mn3 and Mn4 polyhedra. This could possibly indicate

the preferential occupancy of Mn^{3+} in Mn1 and Mn2; this cation is larger than Mn^{4+} , having an ionic radius of 0.645 \AA (Shannon, 1976) and displays the Jahn-Teller effect. On the contrary, Mn3 and Mn4 are more regular and have a

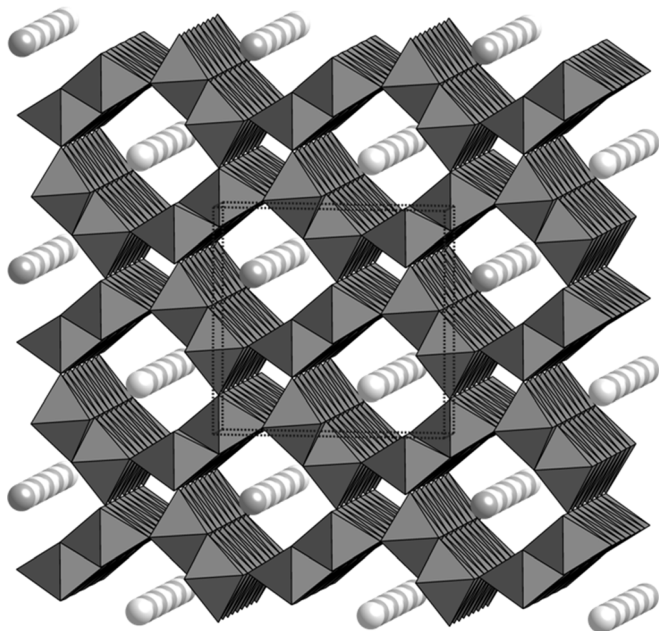


Fig. 4. Crystal structure of ferrihollandite, as seen down [010]. Light grey and dark grey circles are Ba1 and Ba2 sites, respectively.

Table 6. Geometrical parameters of octahedral sites in ferrihollandite.

Site	V (Å ³)	σ ²	λ	Δ (× 10 ³)
Mn1	9.49	39.39	1.012	0.27
Mn2	9.48	40.64	1.012	0.25
Mn3	9.23	33.00	1.010	0.12
Mn4	9.23	32.48	1.010	0.14

smaller size, compatible with a preferential site occupancy by smaller cations, like Mn⁴⁺, with an ionic radius of 0.530 Å (Shannon, 1976). Miura (1986) solved the 2.9 Å crystal structure of hollandite from Gowari Wadhona, India, reporting the angle variance values, that is 34.0 and 30.0 for Mn1 and Mn2, respectively. Also in this case, some geometrical differences occur for the two symmetry-independent Mn sites.

3.3. Tunnel sites

Two independent tunnel sites occur in the crystal structure of ferrihollandite. The tunnel cations fit into distorted prismatic cavities formed by eight oxygen atoms belonging to the octahedral framework; these cavities can host a cation and/or H₂O groups or can be empty. In the studied specimen, the tunnel cations are mainly represented by Ba²⁺ and Sr²⁺, with very minor Na⁺ and K⁺.

The average <Ba–O> distances are 2.915 and 2.891 Å for Ba1 and Ba2, respectively. The unconstrained refinement of the site occupancy factor of Ba1 and Ba2 sites, refining Ba vs. □, gives Ba_{0.22}□_{0.78} and Ba_{0.80}□_{0.20},

respectively. This corresponds to 58 electrons per formula unit (epfu), to be compared with 53.3 epfu calculated from the chemical analysis.

Whereas in previous refinements some authors found satellite sites around the main cation site(s) (*e.g.*, Post *et al.*, 1982; Biagioni *et al.*, 2009a), no significant peaks were observed in the difference-Fourier map of ferrihollandite, even if the highest residual maxima are near Ba2 site.

4. Discussion

4.1. Ordering of A sites in the tunnels

As illustrated above, in addition to the strong sharp Bragg reflections arising from the well-defined octahedral framework of the sub-structure, the reciprocal lattice of ferrihollandite from Vagli displays sharp superstructure reflections doubling the *b* periodicity (Fig. 3). Such sharp reflections are superimposed on diffuse streaks normal to **b***. This probably indicates an ordered arrangement of the A cations within the ferrihollandite tunnels. According to Carter & Withers (2005, and references therein) four factors have been reported as the possible causes for the ordering of A cations in hollandite-type compounds: *i*) intra-tunnel repulsion; *ii*) inter-tunnel interactions between A cations in neighbouring tunnels; *iii*) shielding capacity of the octahedral framework; and *iv*) kinetic effects.

In the crystal structure of ferrihollandite, the two Ba sites have a different site population, allowing an ordered intra-tunnel arrangement avoiding short cation-cation interactions. Consequently, the superstructure reflections could arise from such ordered distribution. The chemical composition of the tunnel sites can be simplified as (Ba_{0.8}Sr_{0.2}); owing to the different site scattering, a first hypothesis can be related to the preferential occupancy of the Ba1 and Ba2 sites by the lighter atom (Sr) and the heavier atom (Ba), respectively. According to Post *et al.* (1982), Ba should be located at the special position 2a (in the sub-structure of hollandite-type structure), whereas Sr should be displaced forming shorter cation–oxygen distances (2.64 Å, predicted using the ionic radii of Shannon, 1976). On the contrary, the <Ba1–O> distance is longer than that observed for Ba2, not agreeing with its occupancy by Sr²⁺.

A careful examination of the refined site scattering values at the two tunnel sites shows a difference between the observed and calculated value (on the basis of electron-microprobe data) of ~ 5 epfu. This value agrees with the electron excess found by Post *et al.* (1982) in ferrihollandite from Sweden, which they attributed to the presence of about 0.5 H₂O groups pfu. If we assume that the electron excess observed in ferrihollandite from Vagli is related to the presence of some additional elements hosted in the tunnels, *i.e.* oxygen belonging to H₂O groups, the amount of H₂O per formula unit would correspond to 0.6 H₂O (~ 1.3 wt%). This value agrees with the first mass loss

observed in the thermogravimetric study, that is ~ 1.5 wt% up to 750 °C. The retention of water up to such a high temperature could seem surprising, owing to the fact that these phases do not contain significant hydroxyl groups, as shown by Potter & Rossman (1979); Bish & Post (1989) reported the water evolution as a function of temperature for a series of tunnel-structure manganese oxides. In particular, they studied the release of water from hollandite (actually ferrihollandite) from Stuur Njuoskes, Sweden; they found a total water loss of 1.72 wt%, with a maximum between 600 and 800 °C, in agreement with the result obtained for ferrihollandite from Vagli. The retention of water up to 750–800 °C may be due to the small size of the free diameter of the tunnels, that is *ca.* 2 Å (according to the definition given by McCusker, 2005) and to the bonds between A cations and H₂O groups. Water can be released only when the crystal structure of hollandite-type compounds collapses, transforming into bixbyite.

The occurrence of an ordered sequence Ba–H₂O–Ba–H₂O may be the reason for the appearance of superstructure reflections, as observed by Turner & Post (1988) for the 3 × 2 tunnel oxide romanechite. Assuming a full occupancy of Ba1 and Ba2 sites, the bond valence sum is 1.33 and 1.42 valence unit (vu), respectively, indicating a strong undersaturation of the tunnel cations. The undersaturation can be an effect of the average position of these sites within the tunnels; another hypothesis agrees with the alternation of (Ba,Sr) and H₂O groups at Ba2 and Ba1 sites, respectively. In this way, the bond valence sum of Ba2 increase up to 1.79 vu, to be compared with an expected value of 1.96 vu. Consequently, the ordered Ba–H₂O–Ba–H₂O sequence would result in a better (Ba,Sr) coordination and would avoid too short cation-cation distances.

In addition to the ordering along **b**, the long-range order between adjacent tunnels seems to be indicated by the sharpness of superstructure reflections. According to Bursill & Grzanic (1980), the charge density of Ba²⁺ is strong enough to overcome the shielding of the octahedral framework, favouring such ordering in barium hollandites.

Finally, kinetic effects should be taken into account. Carter & Withers (2005) showed that cooling rate is important in determining the degree of ordering of the A site cations. Thermochronologic studies (*e.g.* Fellin *et al.*, 2007), based on (U,Th)/He and fission-track ages on apatite and zircon, showed that the Apuan Alps metamorphic rocks cooled from 240 to 110 °C between 11 and 4 Ma. Consequently, after its crystallization, ferrihollandite from Vagli cooled slowly following the *P-T* path of the country rocks.

4.2. Crystal chemistry of ferrihollandite in the frame of Apuan Alps hydrothermalism

The crystallization of ferrihollandite from Vagli is related to the Alpine tectono-metamorphic events and to the circulation of hydrothermal fluids in the “Diaspri” Formation. Montomoli *et al.* (2005) studied the quartz vein system hosted in the “Diaspri” Formation at

Gorfigliano, few kilometres north of Vagli area. Through SEM-EDS analyses, these authors found small amounts of Mn and traces of Fe in the salt residues left after the evaporation of opened fluid inclusions. Massi *et al.* (2008) gave the results of PIXE measurements on fluid inclusions from the same quartz vein systems showing high metal concentrations (Fe, Mn, Sr, Ca, Pb, Zn). The crystal chemistry of ferrihollandite from Vagli is in agreement with the fluid chemistry, owing to its high Fe and Sr content, with respect to other hollandite occurrences.

Enami & Banno (2001) suggested that the large open tunnel in hollandite structure is more suitable for the incorporation of Sr than the piemontite structure. Our data agree with the conclusion of these authors, as the piemontite coexisting with ferrihollandite from Vagli is devoid of Sr, whereas ferrihollandite contains up to 0.20 Sr pfu

5. Summary

This is the first determination of the 5.8 Å superstructure of a natural member of the coronadite group, in the hollandite supergroup. In the mineralogical literature, only two other phases belonging to this group were described with a double *b* (or *c*, according to a tetragonal cell) periodicity, *i.e.* ferrihollandite from Kajlidongri, India (Mukherjee, 1960) and strontiomelane from Praborna, Italy (Meisser *et al.*, 1999). In the priderite group, Szymański (1986) solved the 5.8 Å structure of mannardite.

The crystal structure determination suggests that the lower-charge cations (Fe³⁺, Mn³⁺) are preferentially hosted in Mn1 and Mn2 sites and that the superstructure reflections may result from the ordering of Ba and H₂O groups in the tunnel direction. The occurrence of H₂O groups in the tunnel is suggested by TG-DSC and structural data; this observation is in agreement with Biagioni *et al.* (2013), who stated that minerals belonging to the hollandite supergroup are formally anhydrous although extra-framework water has been reported by various authors (*e.g.*, Nambu & Tanida, 1967; Miura, 1986; Scott & Peatfield, 1986; Post & Bish, 1989).

Acknowledgements: Financial support by MIUR (PRIN 2009 project “Structure, microstructure and properties of minerals”) is acknowledged. The manuscript was handled by the Chief Editor Sergey Krivovichev. The comments of two anonymous referees helped us in improving the paper.

References

- Battaglia, S., Nannoni, R., Orlandi, P. (1977): La piemontite del Monte Corchia (Alpi Apuane). *Atti Soc. Tosc. Sci. Nat., Mem.*, **84**, 174–178.
- Biagioni, C., Orlandi, P., Pasero, M. (2009a): Ankangite from the Monte Arsiccio mine (Apuan Alps, Tuscany, Italy): occurrence,

- crystal structure, and classification problems in cryptomelane group minerals. *Per. Mineral.*, **78**, 3–11.
- Biagioni, C., Orlandi, P., Perchiazzi, N. (2009b): Manganese ores in metamorphic settings: the vein system from Vagli (Apuan Alps, Tuscany, Italy). *Epitome*, **3**, 109.
- Biagioni, C., Capalbo, C., Pasero, M. (2013): Nomenclature tunings in the hollandite supergroup. *Eur. J. Mineral.*, **25**, 85–90.
- Bish, D.L. & Post, J.E. (1989): Thermal behavior of complex, tunnel-structure manganese oxides. *Am. Mineral.*, **74**, 177–186.
- Bonazzi, P., Garbarino, C., Menchetti, S. (1992): Crystal chemistry of piemontites: REE-bearing piemontite from Monte Brugiana, Alpi Apuane, Italy. *Eur. J. Mineral.*, **4**, 23–33.
- Bruker AXS Inc (2004): APEX 2. Bruker advanced X-ray solutions. Madison, Wisconsin, USA.
- Bursill, L.A. & Grzanic, G. (1980): Incommensurate superlattice ordering in the hollandites $Ba_xTi_{8-x}Mg_xO_{16}$ and $Ba_xTi_{8-2x}Ga_{2x}O_{16}$. *Acta Crystallogr.*, **B36**, 2902–2913.
- Cabella, R., Lucchetti, G., Marescotti, P. (1998): Mn-ores from Eastern Ligurian ophiolitic sequences (“Diaspri di Monte Alpe” formation, northern Apennines, Italy). *Trends Mineral.*, **2**, 1–17.
- Capalbo, C. (2013): Minerals of the hollandite supergroup: crystal chemistry and thermal behavior. PhD thesis, University of Pisa, 268 p.
- Carter, M.L. & Withers, R.L. (2005): A universally applicable composite modulated structure approach to ordered $Ba_xM_yTi_{8-y}O_{16}$ hollandite-type solid solutions. *J. Solid St. Chem.*, **178**, 1903–1914.
- Di Sabatino, L. (1967): Su una paragenesi del giacimento manganeseifero di Scortico (Alpi Apuane). *Per. Mineral.*, **36**, 965–992.
- Enami, M. & Banno, Y. (2001): Partitioning of Sr between coexisting minerals of the hollandite- and piemontite-groups in a quartz-rich schist from the Sanbagawa metamorphic belt, Japan. *Am. Mineral.*, **86**, 205–214.
- Fellin, M.G., Reiners, P.W., Brandon, M.T., Wüthrich, E., Balestrieri, M.L., Molli, G. (2007): Thermochronologic evidence for the exhumational history of the Alpi Apuane metamorphic core complex, northern Apennines, Italy. *Tectonics*, **26**, TC6015.
- Fermor, L.L. (1906): Manganese in India. *Trans. Min. Geol. Inst. India*, **1**, 69–131.
- Franceschelli, M., Puxeddu, M., Carcangiu, G., Gattiglio, M., Pannuti, F. (1996): Breccia-hosted manganese-rich minerals of Alpi Apuane, Italy: a marine, redox-generated deposit. *Lithos*, **37**, 309–333.
- Hsu, L.C. & Galli, E. (1973): Origin of the scheelite-powellite series of minerals. *Econ. Mineral.*, **68**, 681–696.
- Keskinen, M. & Liou, J.G. (1979): Synthesis and stability relations of Mn-Al piemontite, $Ca_2MnAl_2Si_3O_{12}(OH)$. *Am. Mineral.*, **64**, 317–328.
- Lucchetti, G., Cortesogno, L., Palenzona, A. (1988): Low-temperature metamorphic assemblages in Mn-Fe ores from Cerchiarra mine (northern Apennines, Italy). *N. Jb. Mineral. Mh.*, **1988**, 367–383.
- Manceau, A., Marcus, M.A., Grangeon, S. (2012): Determination of Mn valence states in mixed-valent manganates by XANES spectroscopy. *Am. Mineral.*, **97**, 816–827.
- Massi, M., Calusi, S., Giuntini, L., Ruggieri, G., Dini, A. (2008): External micro-PIXE analysis of fluid inclusions: test of the LABEC facility on samples of quartz veins from Apuan Alps (Italy). *Nucl. Instrum. Methods Phys. Res.*, **B266**, 2371–2374.
- McCusker & L.B. (2005): IUPAC nomenclature of ordered microporous and mesoporous materials and its application to non-zeolite microporous mineral phases. *Rev. Mineral. Geochem.*, **57**, 1–16.
- Meisser, N., Perseil, E.A., Brugger, J., Chiappero, P.J. (1999): Strontiomelane, $SrMn^{4+}_6Mn^{3+}_2O_{16}$, a new mineral species of the cryptomelane group from St. Marcel – Praborna, Aosta Valley, Italy. *Can. Mineral.*, **37**, 673–678.
- Miura, H. (1986): The crystal structure of hollandite. *Mineral. J.*, **13**, 119–129.
- Montomoli, C., Ruggieri, G., Carosi, R., Dini, A., Genovesi, M. (2005): Fluid source and pressure-temperature conditions of high-salinity fluids in syn-tectonic veins from the Northeastern Apuan Alps (Northern Apennines, Italy). *Phys. Chem. Earth*, **30**, 1005–1019.
- Mukherjee, B. (1960): Space group and cell dimensions of a specimen of hollandite. *Acta Crystallogr.*, **13**, 164–165.
- Nambu, M. & Tanida, K. (1967): Manjiroite, a new manganese dioxide mineral, from Kohare Mine, Iwate Prefecture, Japan. *J. Jpn. Ass. Mineral. Petrol. Econ. Geol.*, **58**, 39–54. (in Japanese).
- Orlandi, P. (1984): Segnalazione di nuove specie mineralogiche da località italiane. *Riv. Mineral. It.*, **2/1984** 33–40.
- Pasero, M. (2005): A short outline of the tunnel oxides. *Rev. Mineral. Geochem.*, **57**, 291–305.
- Perchiazzi, N. & Biagioni, C. (2005): Sugilite e serandite dei Diaspri Auctt. di Vagli (Alpi Apuane). *Atti. Soc. Tosc. Sci. Nat., Mem.*, **110**, 67–71.
- Post, J.E. & Bish, D.L. (1989): Rietveld refinement of the coronadite structure. *Am. Mineral.*, **74**, 913–917.
- Post, J.E., Von Dreele, R.B., Buseck, P. (1982): Symmetry and cation displacements in hollandites: structure refinements of hollandite, cryptomelane and priderite. *Acta Crystallogr.*, **B38**, 1056–1065.
- Potter, R.M. & Rossman, G.V. (1979): The tetravalent manganese oxides: identification, hydration, and structural relationships by infrared spectroscopy. *Am. Mineral.*, **64**, 1119–1218.
- Robinson, K., Gibbs, G.V., Ribbe, P.H. (1971): Quadratic elongation: a quantitative measure of distortion in coordination polyhedra. *Science*, **172**, 567–570.
- Scott, J.D., & Peatfield, G.R. (1986): Mannardite $[Ba \cdot H_2O](Ti_6V^{3+}_2)O_{16}$, a new mineral species, and new data on redledgeite. *Can. Mineral.*, **24**, 55–66.
- Shannon, R.D. (1976): Revised effective ionic radii and systematic studies of interatomic distances in halides and chalcogenides. *Acta Crystallogr.*, **A32**, 751–767.
- Sheldrick, G.M. (2008): A short history of SHELX. *Acta Crystallogr.*, **A64**, 112–122.
- Szymański, J.T. (1986): The crystal structure of mannardite, a new hydrated cryptomelane-group (hollandite) mineral with a doubled short axis. *Can. Mineral.*, **24**, 67–78.
- Turner, S. & Post, J.E. (1988): Refinement of the substructure and superstructure of romanechite. *Am. Mineral.*, **73**, 1155–1161.
- Wilson, A.J.C. ed. (1992): International tables for X-ray crystallography, Volume C: mathematical, physical and chemical tables. Kluwer Academic, Dordrecht, NL.

Received 27 June 2013

Modified version received 18 September 2013

Accepted 23 October 2013